Excitation transfer through open quantum networks: Three basic mechanisms

Lorenzo Campos Venuti and Paolo Zanardi

Institute for Scientific Interchange (ISI), Viale S. Severo 65, I-10133 Torino, Italy and
Department of Physics and Astronomy and Center for Quantum Information Science & Technology, University of Southern California,
Los Angeles, California 90089-0484, USA

A variety of open quantum networks are currently under intense examination to model energy transport in photosynthetic systems. Here, we study the coherent transfer of a quantum excitation over a network incoherently coupled with a structured and small environment that effectively models the photosynthetic reaction center. Our goal is to distill a few basic, possibly universal, mechanisms or effects that are featured in simple energy-transfer models. In particular, we identify three different phenomena: the congestion effect, the asymptotic unitarity, and the staircase effects. We begin with few-site models, in which these effects can be fully understood, and then proceed to study more complex networks similar to those employed to model energy transfer in light-harvesting complexes.

I. INTRODUCTION

The transport of electronic excitations over biological networks of chromophores is the relevant mechanism for the light-harvesting step of photosynthesis.[1–6] Recently, long-lived quantum coherent oscillations have been observed in ultrafast experiments carried out on several biological systems, even at room temperature.[7–12] One of the key features of these exciton-transfer networks is their open nature, namely, that their coupling with the protein vibrational environment is, arguably, the dominant effector of transport in these systems. The interplay of unitary dynamics and the system-bath interaction has been predicted to be beneficial to the network functionality at biological conditions.[13–22] The competition between exciton delocalization and environment-induced relaxation among excitons has been studied for a long time[2–4,6,7,15,18,20] (see also the book[23]). Realistic numerical modeling of these open quantum networks is, to some extent, possible and currently actively pursued in the physical chemistry community.[20,24–33] Nevertheless, the physical chemistry and quantum information community has learned much from simple Markovian models.[14,17,26,32]

In this paper, motivated by the above, we will investigate a few simple yet illuminating models of open quantum networks in order to identify a handful of basic mechanisms or effects that are featured in fully analyzable *toy models* and that may persist for larger, more complex quantum transport networks. In particular, we will focus on coherently coupled qubits subject to dissipation and dephasing and irreversibly connected to an auxiliary quantum system. The role of the latter is to model the reaction center of light-harvesting complexes, where the electronic excitation is separated into an electron and a hole and the charge-transfer stage of photosynthesis begins. Of interest to us is the reaction center of the LH1-RC complexes present in purple bacteria.[1,2,26,34] We will adopt a Markovian master equation of the Lindblad form to describe the overall system dynamics. Different energies, or equivalently time scales, will enter the definition of the Liouville superoperator $\mathcal{L}$. The interplay of these time scales controls the nontrivial phenomenology that we explore in this paper. Finally, singling

out a few intriguing, possibly universal features of such a phenomenological landscape is the goal of the simple calculations presented in this paper.

In the next three sections (II, III, and IV), we will consider different toy models consisting of few sites or chromophores (modeled as quantum two-level systems, or qubits), manifesting particular features, which can be fully understood by analytical calculations. See Fig. 1 for a cartoon picture of the various networks considered. In Sec. V, we consider more realistic networks borrowed from models of light-harvesting complexes. Via numerical simulations, we show that these effects may persist in more realistic systems.

II. THE CONGESTION EFFECT

In exciton and electron transfer events, there can be delays in energy transport due to the time scales of the biological process. A particular element might be shut down while transport takes place, effectively making an exciton or electron wait until the transport is possible.[35] In the following section, we describe this phenomenon in model systems and characterize it as the *congestion effect*.

In the standard modeling of incoherent (and irreversible) transfer of excitations from one site to another, the Förster electromagnetic coupling mechanism permits the transfer of populations at a given rate γ. If the dynamics is described using a Lindblad form $\dot{\rho} = \mathcal{L}_L(\rho)$, where $\mathcal{L}_L(X) = LXL^\dagger - \{L^\dagger L, X\}/2$, this can be accounted for by a jump operator of the form $L = \sqrt{\gamma}\sigma^- \otimes \sigma^+$, where $\sigma^\pm$ are Pauli ladder operators. In the actual transfer process, excitations may spread on complicated pathways, interact with external modes, and so on. In most cases, the detailed microscopical process that gives rise to such a transfer term are to a large extent unknown, and this motivates the simple phenomenological Lindbladian given above. On the basis of the detailed balance condition, this one-way transfer must always be accompanied by the reverse process, which transfers excitations in the opposite direction (see, e.g., Ref. 36). The backward transfer rate γ_{back} satisfies approximately $\gamma_{\text{back}}/\gamma \approx e^{-\Delta F/kT}$. Here, aiming at simplicity, we will neglect the effect of backward process; in other words,
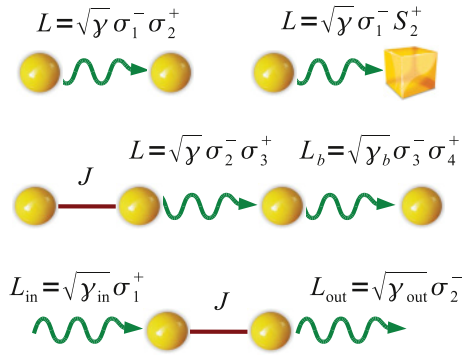
FIG. 1. (Color online) Summary of the toy networks analyzed analytically in Secs. II and III.

we will assume that the free-energy difference ΔF is large as compared to the temperature.

Later on, we will model that part of light-harvesting complexes where the exciton is finally transferred to the reaction center via a one-way process as done elsewhere in the literature.[14,15,17,18,26,28,29,32] However, we will move from this simple phenomenological picture by adding different layers of complexity. More precisely, we will give the reaction center a richer structure allowing it to accommodate for more than one exciton and/or we will split the trapping process in two by adding an extra, fictitious site, with the aim of introducing another time scale in the trapping process (γ_b^{-1} in Fig. 1).

In this section, we explore possible *congestion* effects that arise from the dependence of the transfer rate on the number of excitations involved, in the same way traffic flow might be inversely proportional to the number of vehicles present on roads.

Incoherent transfer I: $\bullet \overset{\gamma}{\rightsquigarrow} \bullet$. Before turning to analyze the possible implementations and consequences of such an effect, let us summarize the Lindblad operators for incoherent Förster transfer among two sites $L = \sqrt{\gamma}\sigma_1^-\sigma_2^+$. This process can be pictorially visualized by the following diagram: $\bullet \overset{\gamma}{\rightsquigarrow} \bullet$ (see also Fig. 1). The quantum master equation is given simply by $\dot{\rho} = \mathcal{L}_L(\rho)$. We denote by $\mathfrak{n}$ the population operator satisfying $\mathfrak{n}|\eta\rangle = \eta|\eta\rangle$ with $\eta = 0,1$, and by n its possibly time-dependent expectation value for excitations, i.e., $n = \langle\mathfrak{n}\rangle := \mathrm{tr}(\mathfrak{n}\rho)$. Since the effect of the Lindbladian is to transfer a particle from site 1 to site 2, the total number operator is a conserved quantity. We therefore obtain a differential equation for the population in the following way: first note that $\dot{n}_i = \mathrm{tr}(\mathfrak{n}_i\dot{\rho}) = \mathrm{tr}[\mathfrak{n}_i\mathcal{L}_L(\rho)]$. Given that $n_1 + n_2 = n_{\mathrm{tot}}$ is constant in time, it suffices to analyze the population of site 1, $\dot{n}_1 = -\gamma n_1 + \gamma\langle\mathfrak{n}_1\mathfrak{n}_2\rangle$. Now note that, in the single-particle sector, $\mathfrak{n}_{\mathrm{tot}} = 1$, $\langle\mathfrak{n}_1\mathfrak{n}_2\rangle = 0$ (to see this, use $\mathfrak{n}_{\mathrm{tot}}^2 = \mathfrak{n}_{\mathrm{tot}} + 2\mathfrak{n}_1\mathfrak{n}_2$), leading to a transport equation $\dot{n}_1 = -\gamma n_1$ that can be readily solved for the population at sites 1, $n_1(t) = e^{-\gamma t}n_1(0)$, and, 2, $n_2(t) = n_2(0) + (1 - e^{-\gamma t})n_1(0)$. The jump operator achieves precisely what we expected: the population in site 1 decreases exponentially at a rate γ and the population of site 2 increases accordingly. The same result could have been obtained by solving the (16-dimensional) differential equation for the full density matrix. Starting at time zero with

$\rho(0) = \{\rho_{i,j}\}$, the time-evolved density matrix $\rho(t)$ in the basis $\{|11\rangle, |10\rangle, |01\rangle, |00\rangle\}$ is

$$\begin{pmatrix} \rho_{1,1} & e^{-\gamma t/2}\rho_{1,2} & \rho_{1,3} & \rho_{1,4} \\ e^{-\gamma t/2}\rho_{2,1} & e^{-\gamma t}\rho_{2,2} & e^{-\gamma t/2}\rho_{2,3} & e^{-\gamma t/2}\rho_{2,4} \\ \rho_{3,1} & e^{-\gamma t/2}\rho_{3,2} & (1-e^{-\gamma t})\rho_{2,2} + \rho_{3,3} & \rho_{3,4} \\ \rho_{4,1} & e^{-\gamma t/2}\rho_{4,2} & \rho_{4,3} & \rho_{4,4} \end{pmatrix}.$$

It is interesting to note, in passing, that for some entangled initial states, the asymptotic density matrix $\rho(t \to \infty)$ is still entangled. The process $\mathcal{L}_L$ can not, however, create entanglement.

Incoherent transfer II: $\bullet \rightsquigarrow \square$. We now allow the second site to accommodate for more than just one exciton. Accordingly, we replace the second qubit with a larger $d = 2s + 1$ dimensional space. One can then act on the second site with irreducible spin s representation of SU(2) operators.

For this case, we can model a particle-conserving transfer process with a jump operator given by $L = \sqrt{\gamma}\sigma_1^- S_2^+$, where S_2^+ is a raising operator of the irreducible spin s representation of SU(2). The population at site 2 is $\mathfrak{N}_2 = S_2^z + s\mathbb{1}$. Once again, since the total particle number $\mathfrak{n}_{\mathrm{tot}} = \mathfrak{n}_1 + \mathfrak{N}_2$ is conserved in a given particle sector, one has $\mathfrak{n}_{\mathrm{tot}}(t) = n_{\mathrm{tot}}$. We then obtain the following differential equation for population at site 1: $\dot{n}_1 = -\gamma\langle\mathfrak{n}_1 S_2^- S_2^+\rangle$. By noting that $S_2^- S_2^+ = (\mathfrak{N}_2 + 1)(2s - \mathfrak{N}_2)$, and employing $\mathfrak{N}_2 = n_{\mathrm{tot}} - \mathfrak{n}_1$, $\mathfrak{N}_2^2 = n_{\mathrm{tot}}^2 - 2n_{\mathrm{tot}} - 1 + 2\mathfrak{n}_1$, and $\mathfrak{n}_1^2 = \mathfrak{n}_1$, we obtain an explicit differential equation for n_1:

$$\dot{n}_1 = -\gamma n_{\mathrm{tot}}[(2s + 1) - n_{\mathrm{tot}}]n_1,$$
$$n_1 + N_2 = n_{\mathrm{tot}}.$$

Excitation transfer now occurs at an effective rate, which depends on the total population: $\gamma_{\mathrm{eff}} = \gamma n_{\mathrm{tot}}[(2s + 1) - n_{\mathrm{tot}}]$. Note that $0 \leqslant n_{\mathrm{tot}} \leqslant 2s + 1$ and, correctly, $\gamma_{\mathrm{eff}}(n_{\mathrm{tot}} = 0) = \gamma_{\mathrm{eff}}(n_{\mathrm{tot}} = 2s + 1) = 0$, i.e., no transfer takes place when the network is either completely empty or completely full. The maximum transfer rate is attained when the condition $n_{\mathrm{tot}} = (2s + 1)/2$ is satisfied. The lesson we get from this slightly modified example is that transferring excitations to an object with more than just two levels is likely to result in a population-dependent transfer rate.

Interplay between coherent hopping and transfer: $\bullet \overset{J}{\leftrightarrow} \bullet \overset{\gamma}{\rightsquigarrow} \bullet \overset{\gamma_b}{\rightsquigarrow} \bullet$. We will further illustrate the concept above by considering a variation on the theme. We consider a coherent-hopping Hamiltonian on four sites of the form $H = (J/2)(\sigma_1^-\sigma_2^+ + \mathrm{H.c.})$ that acts on the first two sites. The excitations are transferred irreversibly from site 2 to site 3 via a quantum jump operator $L = \sqrt{\gamma}\sigma_2^-\sigma_3^+$ and, subsequently, from site 3 to site 4 with $L_b = \sqrt{\gamma_b}\sigma_3^-\sigma_4^+$. J is the coherent coupling strength. In the following, we explore the interplay between the two incoherent transfer rates γ and γ_b. Let us focus on the population at site 3, $n_3(t)$. The effect of γ_b is that of removing excitation population from site 3. However, when γ_b becomes large, excitations are rapidly transferred to site 4, inhibiting the effect of L_b [$\mathcal{L}_b(\rho) \to 0$]. This results in a nontrivial nonmonotonic effect as a function of γ_b. This feature can be visible only if we have at least two particles in the network. Let us then consider the following initial (pure) state with excitations localized at sites 1 and 2: $|1,1,0,0\rangle$. As shown

in Fig. 3, in this case, the time evolution of the populations takes the following form:

$$n_1(t) = C_1 e^{-\gamma t} + C_2 e^{-\gamma t/2} + C_3(t) e^{-t\gamma_b}$$
$$+ C_4 e^{-t(\gamma+\omega)/2} + C_5 e^{-t(\gamma-\omega)/2},$$

$$n_2(t) = C_1' e^{-\gamma t} + C_2' e^{-\gamma t/2} + C_3'(t) e^{-t\gamma_b}$$
$$+ C_4' e^{-t(\gamma+\omega)/2} + C_5' e^{-t(\gamma-\omega)/2},$$

$$n_3(t) = 1 + B_1(t) e^{-t\gamma_b} + B_2 e^{-t\gamma} + B_3 e^{-t\gamma/2}$$
$$+ B_4 e^{-t(\gamma+\omega)/2},$$

$$n_4(t) = \frac{\gamma(1 - e^{-t\gamma_b}) - \gamma_b(1 - e^{-t\gamma})}{\gamma - \gamma_b},$$

where C_i, C_i', B_i are only functions of J, γ, γ_b, and C_3, C_3', B_1 are functions of time as well. Finally, $\omega = \sqrt{\gamma^2 - 4J^2}$, resulting in an imaginary eigenvalue of the Liouvillian for $2|J| > \gamma$. This, in turn, shows up in an oscillating behavior of the populations as a function of time. In Fig. 2, the behavior of population 3 as a function of time and γ_b is plotted for the given values of J and γ. For large values of t, one can observe a nonmonotonic behavior as a function of γ_b emphasized in the bottom panel of Fig. 2. This behavior can be qualitatively understood as follows. Consider the behavior of n_3 as a function of γ_b for a large fixed time $\tilde{t}$. Since the effect of γ_b is that of taking away particles from site 3, n_3 first decreases when γ_b is increased from zero at fixed $\tilde{t}$. Anyway, if γ_b is further increased, excitations are taken away at a faster rate and transferred to site 4. This means that, at the fixed time $\tilde{t}$, site 4 tends
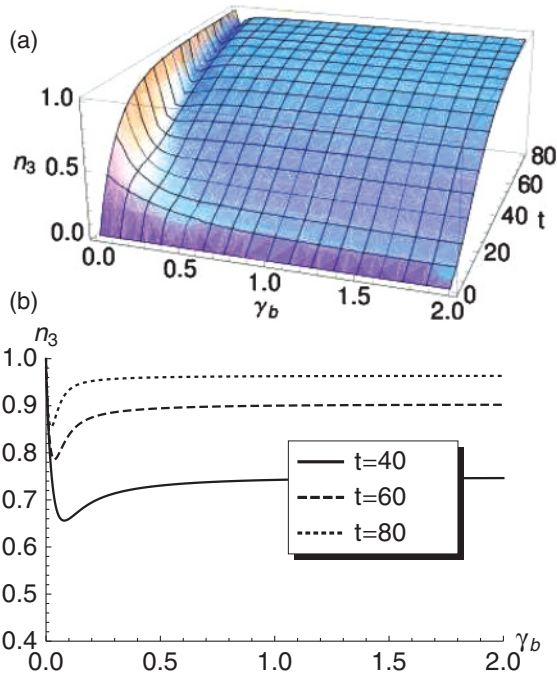

FIG. 2. (Color online) (a) 3D plot of the population n_3 for the case described in Sec. II, as a function of time and γ_b. In this model, the initial state has two excitations at sites 1 and 2: $|1,1,0,0\rangle$. The parameters for the model are $J = 1$, $\gamma = 0.1$. (b) Slices of the same plot at different times are shown. The nonmonotonic behavior of the population as a function of the rate γ_b is evident at small values of it.
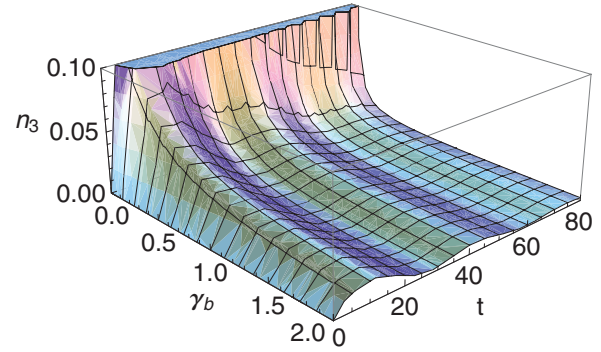

FIG. 3. (Color online) 3D plot of n_3 as a function of time and γ_b. Initial state has one excitation at site 1: $|1,0,0,0\rangle$. Parameters are $J = 1$, $\gamma = 0.05$.

to get full for large γ_b, thus inhibiting the effect of L_b. Population n_3 then increases with γ_b. When γ_b is further increased, site 4 becomes effectively full and L_b is turned off, the population becomes then independent of γ_b, and n_3 saturates.

For the sake of completeness, we also consider the solution with one excitation localized at site 1, i.e., $|1,0,0,0\rangle$ at time $t = 0$. In this case, the time dependence of the populations is

$$n_1(t) = \frac{e^{-t\gamma/2}}{\omega^3} \left[-2J^2\omega + (\gamma^2 - 2J^2)\omega \cosh\left(\frac{t\omega}{2}\right) \right.$$
$$\left. + \gamma\omega^2 \sinh\left(\frac{t\omega}{2}\right) \right],$$

$$n_2(t) = \frac{2J^2 e^{-t\gamma/2}}{\omega^2} \left[\cosh\left(\frac{t\omega}{2}\right) - 1 \right],$$

$$n_3(t) = A_1 e^{-t\gamma_b} + A_2 e^{-t\gamma} + A_3 e^{-t(\gamma+\omega)/2} + A_4 e^{-t(\gamma-\omega)/2},$$

$$n_4(t) = 1 - \sum_{i=1}^{3} n_i(t),$$

where A_i are time-independent functions of the parameters. One can see in Fig. 3 that the nonmonotonic behavior of n_3 as a function of γ_b is, for this initial condition, absent. As expected, since in the network there are no excitations enough to fill the reaction center, the "congestion effect" is now absent.

III. THE STAIRCASE EFFECT

In this section, we explore the situation where excitons are fed into a quantum network at a given constant rate γ_{in} and are extracted at a rate γ_{out}. This model can be justified by the fact that some photosynthetic complexes such as purple bacteria and green-sulfur bacteria[37] live in low-light conditions. The electron-transfer event that occurs in the reaction center is a process that takes place in the order of picoseconds. We therefore take the common practice of modeling the reaction center as an incoherent trap.[14]

Injection-extraction: $\overset{\gamma_{\text{in}}}{\leadsto} \bullet \overset{J}{\leftrightarrow} \bullet \overset{\gamma_{\text{out}}}{\leadsto}$. Here, we consider the simplest model for the injection and extraction of an exciton. The model corresponds to two sites coupled coherently via

the hopping Hamiltonian $H = (J/2)(\sigma_1^- \sigma_2^+ + \sigma_1^+ \sigma_2^-)$. Aside from the coherent evolution term, an incoherent injection of excitons is given by a jump operator $L_{in} = \sqrt{\gamma_{in}}\sigma_1^+$, which injects particles at a rate γ_{in} and a corresponding incoherent extraction term $L_{out} = \sqrt{\gamma_{out}}\sigma_2^-$.

The corresponding 16×16 Lindblad superoperator matrix can be diagonalized. A complex eigenvalue with a nonzero imaginary part gives rise to oscillating behavior in the populations when $|\gamma_{in} - \gamma_{out}| < 2|J|$.

Let us first concentrate on the asymptotic state of the evolution $\rho(t \to \infty)$. By solving $\mathcal{L}_{tot}(\rho) = 0$, one realizes that the asymptotic state is unique and independent of the initial state. Although this feature is expected in natural physical systems and follows, for instance, from the detailed balance hypothesis, it is not necessarily satisfied in our simple toy models (see, e.g., Sec. II).

In the standard basis $\{|1,1\rangle, |1,0\rangle, |0,1\rangle, |0,0\rangle\}$, the explicit expression of the asymptotic state is

$$\rho(\infty) = \frac{1}{(\gamma_{in} + \gamma_{out})(J^2 + \gamma_{in}\gamma_{out})}$$

$$\times \begin{pmatrix} \frac{J^2\gamma_{in}^2}{(\gamma_{in}+\gamma_{out})} & 0 & 0 & 0 \\ 0 & \frac{\gamma_{in}\gamma_{out}[J^2+(\gamma_{in}+\gamma_{out})^2]}{(\gamma_{in}+\gamma_{out})} & iJ\gamma_{in}\gamma_{out} & 0 \\ 0 & -iJ\gamma_{in}\gamma_{out} & \frac{J^2\gamma_{in}\gamma_{out}}{(\gamma_{in}+\gamma_{out})} & 0 \\ 0 & 0 & 0 & \frac{J^2\gamma_{out}^2}{(\gamma_{in}+\gamma_{out})} \end{pmatrix}.$$

The only nonvanishing correlations are $\langle \sigma_1^z \sigma_2^z \rangle$, $\langle \sigma_1^z \rangle$, and $\langle \sigma_2^z \rangle$. Thus, this state is separable but has nonvanishing classical correlations: $\langle \sigma_1^z \sigma_2^z \rangle - \langle \sigma_1^z \rangle \langle \sigma_2^z \rangle \neq 0$. Equivalently, the asymptotic state is a classical mixture of states with definite populations.

Having $\rho(\infty)$, we can compute the asymptotic populations:

$$n_1(\infty) = \frac{\gamma_{in}(J^2 + \gamma_{in}\gamma_{out} + \gamma_{out}^2)}{(\gamma_{in} + \gamma_{out})(J^2 + \gamma_{in}\gamma_{out})}, \tag{1}$$

$$n_2(\infty) = \frac{\gamma_{in}J^2}{(\gamma_{in} + \gamma_{out})(J^2 + \gamma_{in}\gamma_{out})}. \tag{2}$$

A few simple facts can be directly seen from Eqs (1) and (2). First, for small γ_{in}, populations deviate by $O(\gamma_{in})$ from zero; vice versa, for γ_{out}, small populations deviate by $O(\gamma_{out})$ from one. Instead, when J is small, excitations get loaded at site 1 but take a long time to reach site 2 so that $n_1 = 1 - O(J^2)$, $n_2 = O(J^2)$. Finally, for very large J, both populations tend to $n_1 \simeq n_2 = \gamma_{in}/(\gamma_{in} + \gamma_{out}) + O(J^{-2})$.

Let us now turn to the dynamics and consider first the most interesting case, namely, when the initial state is the empty state $|0,0\rangle$. A typical result is shown in Fig. 4. An interesting feature clearly emerges: when population n_1 increases, n_2 stays almost constant and vice versa. Such a feature is particularly evident in the parametric plot. In Fig. 4(b), we also stressed another peculiarity of this process: the time needed to increase a given population when the other is constant (i.e., the horizontal and vertical steps between two red dots in Fig. 4) is always the same. We call T_0 this new, emerging, time scale. The description of the entire process then is the following. First particles are injected at site 1 and population at site 2 stays zero until a time $T_0/2$. Next, for $T_0/2 < t < 3/2T_0$, the situation is reverted and population 2
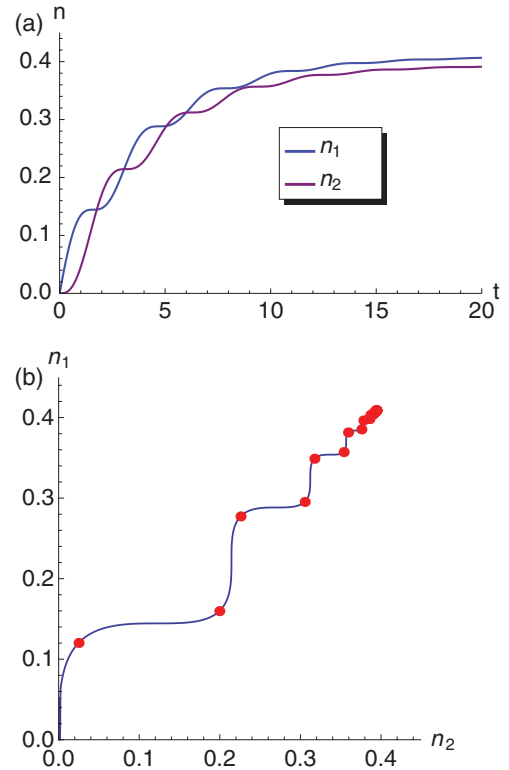

FIG. 4. (Color online) Parameters are $J = 2$, $\gamma_{in} = 0.2$, and $\gamma_{out} = 0.3$, and initial state is $|0,0\rangle$. (a) Plot of the populations as a function of time. (b) Parametric plot with same parameters. The red dots correspond to times given by $T_n = (1/2 + n)T_0$, $T_0 = 2\pi/\omega$ ($n = 1, 2, \ldots$) and the correct frequency is $\omega = \sqrt{4J^2 - (\gamma_{in} - \gamma_{out})^2}$. As explained in the text using general arguments, $T_0 = O(J^{-1})$.

increases while population 1 remains constant. The process continues in this fashion until an asymptotic state is reached. Given the shape of the curve in Fig. 4, we refer to this situation as the "staircase effect." The emerging time scale can be given a physical interpretation considering the limit when both injection and extraction rates are very small. In this case, the dominant process is that dictated by the Hamiltonian H, which represents an excitation hopping back and forth between sites 1 and 2. The period of this oscillation is inversely proportional to the energy-level difference ΔE and is therefore of order J^{-1} [in math, $T_0 \approx 2\pi/\Delta E = O(J^{-1})$]. It is also clear that the populations $n_1(t), n_2(t)$ must increase from zero to reach the asymptotic values given in Eqs. (1) and (2). The staircase effect is then an interplay between coherent oscillations and increase of $n_1(t), n_2(t)$. It is, however, a very peculiar interplay, namely, one in which when $n_1(t)$ grows, $n_2(t)$ stays constant and vice versa. The first part of the curve in Fig. 4, namely, for $0 < t < T_0/2$, can be understood with simple arguments. During this time window, the population at site 1 grows, but any disturbance needs a time $T_0/2$ to reach the second site where, correspondingly, the population stays zero. It would be interesting to see whether an extension of the methods of Ref. 19 not restricted to the zero- or one-particle sector allows us to obtain a kinetic rate equation for the populations n_1, n_2 in this setting. Such a kinetic rate equation would convey a simple classical
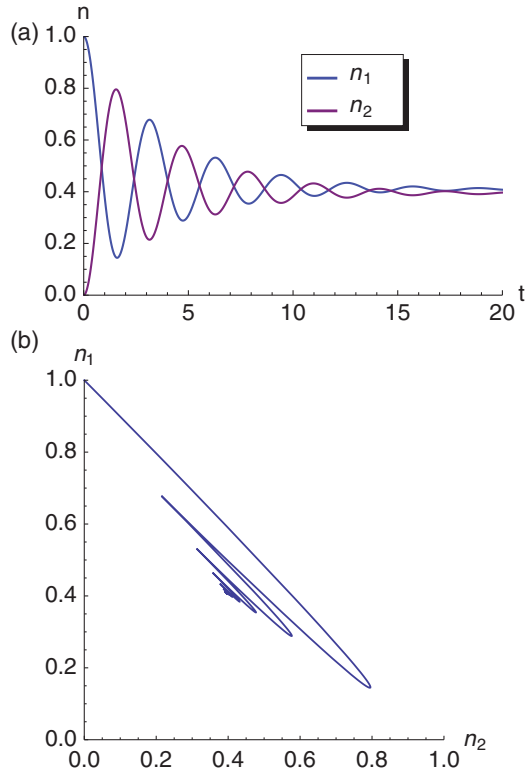
FIG. 5. (Color online) Parameters are $J = 2$, $\gamma_{\text{in}} = 0.2$, $\gamma_{\text{out}} = 0.3$, and initial state is $|1,0\rangle$. (b) Parametric plot with same parameters.

description for the peculiar interplay between "oscillations" and "growth," which gives rise to the steplike behavior of Fig. 4.

In general, if we substitute the two sites with an open chain of length L, we expect (at least for small γ_{in}, γ_{out}) that T_0 will be the time needed for the excitations to travel from one side of the chain to the other, i.e., $T_0 \approx L/v$, where v is the velocity of quasiparticles. Of course, this picture can be correct only as long as a quasiparticle description applies (cf. Sec. V C).

Let us now consider the injection-extraction dynamics with an initial state $|1,0\rangle$, i.e., at time zero the injection site is occupied. A typical (in the oscillating regime) scenario is shown in Fig. 5. Starting with an initial state $|0,1\rangle$, the situation is almost identical with n_1 and n_2 interchanged. In fact, one can show that, for initial states with one definite excitation, populations at any time satisfy the following duality relation:

$$n_1(\gamma_{\text{in}}, \gamma_{\text{out}}) = 1 - n_2(\gamma_{\text{out}}, \gamma_{\text{in}}).$$

As previously explained, the asymptotic populations do not depend on the initial populations and are still given by Eqs. (1) and (2). The parametric plot in Fig. 5(b) shows that, with this initial condition, the staircase effect is not present.

Three-site injection-extraction: $\overset{\gamma_{\text{in}}}{\rightsquigarrow} \bullet \overset{J}{\leftrightarrow} \bullet \overset{J}{\leftrightarrow} \bullet \overset{\gamma_{\text{out}}}{\rightsquigarrow}$. A slight generalization of the above idea is given by a three-site chain with injection on the first site and extraction on the third. For simplicity, we consider a uniform chain with equal couplings $J_{12} = J_{23} = J$. In this case, the asymptotic populations are

given by

$$n_1(\infty) = \frac{\gamma_{\text{in}}(J^2 + \gamma_{\text{in}}\gamma_{\text{out}} + \gamma_{\text{out}}^2)}{(\gamma_{\text{in}} + \gamma_{\text{out}})(J^2 + \gamma_{\text{in}}\gamma_{\text{out}})},$$

$$n_2(\infty) = \frac{\gamma_{\text{in}}(J^2 + \gamma_{\text{out}}^2)}{(\gamma_{\text{in}} + \gamma_{\text{out}})(J^2 + \gamma_{\text{in}}\gamma_{\text{out}})},$$

$$n_3(\infty) = \frac{\gamma_{\text{in}}J^2}{(\gamma_{\text{in}} + \gamma_{\text{out}})(J^2 + \gamma_{\text{in}}\gamma_{\text{out}})}.$$

Note that populations n_1 and n_3 are the same as n_1, n_2 in the previous two-site case. Starting from the totally empty state, the asymptotic state is reached in a similar manner as in the two-site case. In particular, the parametric plot of the injection and extraction sites $[n_1(t), n_3(t)]$ displays a staircase shape exactly as in the two-site case. As we will show in Sec. V C, this feature survives even in a longer chain, and is to some extent resistant to small static diagonal disorder and dephasing.

IV. ASYMPTOTIC UNITARITY

Another effect we want to study is the possibility that a coherent dynamics (or subdynamics) may emerge out of a dissipative or partly incoherent dynamics. To make things more clear, let us immediately discuss the simplest example showing this feature.

Hopping and transfer: $\bullet \overset{J}{\leftrightarrow} \bullet \overset{\gamma}{\rightsquigarrow} \bullet$. The model consists of three sites (qubits). On the first two sites acts a coherent hopping of the form $H = (J/2)(\sigma_1^-\sigma_2^+ + \sigma_1^+\sigma_2^-)$. On top of that, particles are transferred irreversibly from site 2 to site 3 via a jump operator given by $L = \sqrt{\gamma}\sigma_2^-\sigma_3^+$. It is clear that, if a particle sits at site 3, the incoherent part of the dynamics is not effective, that is, $\mathcal{L}_L[\rho_{12} \otimes |1\rangle\langle 1|] = 0$. If we start with an initial state $|1,1,0\rangle$ with sites 1 and 2 occupied and site 3 empty, for effect of the dynamics, site 3 will get populated at a rate γ, and on the first two sites there will remain one particle coherently hopping back and forth. By this we mean that, for a sufficiently large time, the evolved state will be similar to a coherent evolution: $\rho(t) = e^{t\mathcal{L}_{\text{tot}}}[\rho] \simeq e^{-itH}\tilde{\rho}e^{itH} =: \tilde{\rho}(t)$. For what concerns the state $\tilde{\rho}$, we only know that it will contain two particles; it can be obtained by evolving back unitarily $\rho(t)$, i.e.,

$$\tilde{\rho} = \lim_{t \to \infty} e^{itH}\rho(t)e^{-itH}.$$

Indeed, if the dynamics becomes unitary, the above limit is well defined. Notice that $\tilde{\rho}$ is nothing but the stationary solution of the original master equation in the interaction picture associated with H. The same reasoning can be done for the subsystem consisting on sites 1 and 2, i.e., we can define $\tilde{\rho}_{1,2}$ by evolving back unitarily $\rho_{1,2}(t)$. Since H does not act on site 3, we have $\tilde{\rho}_{1,2} = \text{tr}_3\tilde{\rho}$. An explicit computation confirms that $\tilde{\rho} = \tilde{\rho}_{1,2} \otimes |1\rangle\langle 1|$, i.e., in the equivalent unitary dynamics, one particle sits at site 3. The explicit form of $\tilde{\rho}_{1,2}$ in the standard basis is

$$\tilde{\rho}_{1,2} = \frac{1}{2(J^2 + \gamma^2)} \begin{pmatrix} 0 & 0 & 0 & 0 \\ 0 & J^2 + 2\gamma^2 & -iJ\gamma & 0 \\ 0 & iJ\gamma & J^2 & 0 \\ 0 & 0 & 0 & 0 \end{pmatrix}.$$

This state is a quantum superposition of one-particle states with $n_1 = 1/2 + \gamma^2/2(J^2 + \gamma^2)$ and $n_2 = 1/2 - \gamma^2/2(J^2 + \gamma^2)$.

What are the possible indicators of asymptotic unitarity? Since the purity is constant under unitary evolution, one possibility is to look at the purity of the total system or of some part of it. The time derivative of such a quantity will then be close to zero for approximate unitary evolution. Since for Lindbladian evolution the purity derivative is $\partial_t \text{tr}(\rho^2) = 2\text{tr}[\rho(t)\mathcal{L}_{\text{tot}}(\rho)]$, this definition has the advantage of being numerically stable. In our toy model, we have

$$
\text{tr}\{[\rho_{1,2}(t)]^2\}
$$

$$
= \text{tr}[\rho^2] = 1 - \frac{J^2}{2(J^2 + \gamma^2)}
$$

$$
+ \frac{-2e^{-\gamma t}[J^2 + \gamma^2 + \gamma^2 \cos(Jt)] + e^{-2\gamma t}(3J^2 + 4\gamma^2)}{2(J^2 + \gamma^2)}.
$$

Unfortunately, the purity tends to a constant whenever the solution tends to a constant, as happens, for instance, along the natural process reaching the asymptotic state. In other words, the smallness of the purity derivative is a necessary but not sufficient condition for asymptotic unitarity.

Another possibility is to measure some distance between the actual state and the one obtained with unitary evolution: $\|\rho(t) - \tilde{\rho}(t)\|$. Once again, we might as well restrict to a particular subsystem. Using the operator norm, the result for our toy model is particularly simple and illuminating:

$$
\|\rho(t) - \tilde{\rho}(t)\| = \|\rho_{1,2}(t) - \tilde{\rho}_{1,2}(t)\| = e^{-\gamma t}.
$$

This confirms our initial intuition: the dynamics becomes unitary at a rate γ. This approach has a very clear meaning, but has the disadvantage of being computationally demanding as it requires the computation of a matrix norm and the evaluation of $\tilde{\rho}(t)$. A simpler alternative is the following.

Consider the spectral representation of the Hamiltonian $H = \sum_n E_n |n\rangle\langle n|$. If the total evolution becomes similar to a unitary evolution, the matrix elements of the density matrix in the eigenbasis $|n\rangle$ evolve in timelike phases:

$$
\langle n|\rho(t)|m\rangle \simeq \langle n|\tilde{\rho}(t)|m\rangle = e^{-it(E_n - E_m)}\langle n|\tilde{\rho}|m\rangle.
$$

In our model, the eigenbasis of the two-site Hamiltonian is $\{|0,0\rangle, |1,1\rangle, |\psi^\pm\rangle = (|1,0\rangle \pm |0,1\rangle)/\sqrt{2}\}$. For instance, one can show that

$$
\langle\psi^-|\rho_{1,2}(t)|\psi^+\rangle = \frac{\gamma}{iJ + \gamma}[e^{-t\gamma} - \cos(Jt) - i\sin(Jt)].
$$

Pictorially, the parametric plot of the real and imaginary parts of this matrix element folds on a circle (of radius $\gamma/\sqrt{J^2 + \gamma^2}$) after a time γ^{-1} (see Fig. 6).

This method to mark the appearance of asymptotic unitarity, as well as the study of the distance $\|\rho(t) - \tilde{\rho}(t)\|$, has a major advantage with respect to those based on $\dot{\rho}(t)$. Namely, it allows us to discriminate between approximate unitary evolution and the usual reach of an asymptotic state for which $\dot{\rho} = 0$.

We would like to end this section by stressing the (almost obvious) relation of asymptotic unitarity with the quantum-information concept of noiseless or decoherence-free subspace and system.[38] The quantum networks considered in this paper
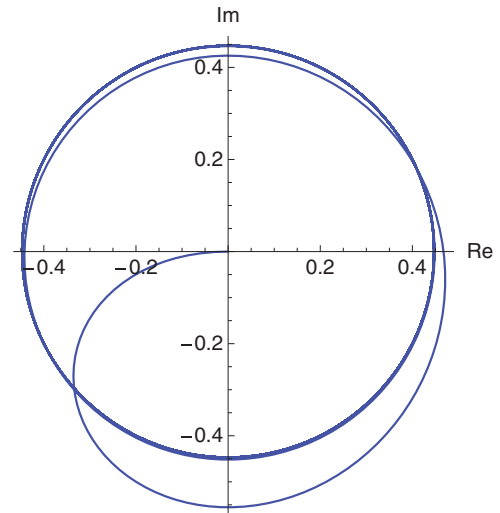

FIG. 6. (Color online) Parametric plot of real and imaginary part of $\langle\psi^-|\rho_{1,2}(t)|\psi^+\rangle$ as a function of time for the model considered in the text. Parameters are $J = 2, \gamma = 1$.

are of hybrid type, namely, some of the intersite couplings are coherent, i.e., hopping, and others are incoherent, i.e., irreversible transfer described by L. On the other hand, the dynamics restricted to the range of the projection $P := \mathbb{1}_{12} \otimes |1\rangle\langle 1|$ is unitary because, as noticed in the above, $\mathcal{L}_L(P\rho P) = 0$. This means that the range of P is indeed a decoherence-free subspace. Now the dynamics is such that, for appropriate initial conditions, $\lim_{t\to\infty} n_3(t) = 1$ or equivalently $\lim_{t\to\infty} \|P\rho(t)P - \rho(t)\| = 0$. This means that the asymptotic state belongs to the range of P, which in turn implies the unitary nature of the long-time dynamics.

V. TOY MODELS FOR PHOTOSYNTHETIC COMPLEXES

In this section, we want to check if and how the effects studied so far can survive in more realistic networks. Specifically, we will consider models that can be relevant for the description of energy transfer in photosynthetic systems. Similar simple modelizations of photosynthetic systems are currently under intense investigation (see, e.g., Refs. 13, 15, 18, 19, and 26). Differently from most of the current literature, here we want to analyze the effect that multiexciton configurations can have on the transfer dynamics. To this end, we will consider the dynamics in the whole Liouville space and not restricted to the zero- and one-exciton sectors as usually done. This requirement results in a computational cost exponentially large in the system size (as opposed to the standard linear growth), which effectively limits the size of the network that can be efficiently simulated to very short ones.

For the analysis of the congestion effect and asymptotic unitarity, we will use the network configuration of the LH1 complex, which is made of 32 bacteriochlorophyll units, limited, however, to a very small ring ($L = 4$ sites). We have tried to incorporate in our short networks most of the features that are present in the actual LH1 complex,[39,40] so that our toy models are effectively a scaled-down version of the actual LH1 complex.
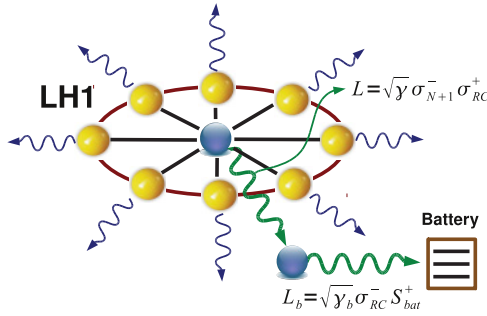
FIG. 7. (Color online) Toy model for LH1 complexes. N particles on the ring interact via dimerized nearest-neighbor hopping constants $t_{i,i+1} = t[1 + \delta(-1)^i]$. Each of these particles can hop to the central site $[(N + 1)\text{th}]$ with hopping constant J. The central site transfers excitations incoherently to the reaction center via $L = \sqrt{\gamma}\sigma_{N+1}^-\sigma_{RC}^+$. The reaction center itself is connected to a $(2s + 1)$-dimensional "battery" via $L_b = \sqrt{\gamma_b}\sigma_{RC}^- S_{\text{bat}}^+$. The effect of external degrees of freedom is schematized by incoherent dissipation and dephasing processes (thin, blue, wavy lines). In actual LH1 complexes, the sites on the ring are bacteriochlorophylls, and $N = 32$.

A. Congestion effect

Our motivation for the study of the "congestion effect" originated from a careful analysis of the structure of the reaction center in LH1-RC complexes. In most photosynthetic bacteria, photons are captured by light-harvesting antennae where a particle-hole exciton is created and carried to the reaction center (RC) where eventually a redox reaction takes place[1]. In the LH1-RC complexes present in purple bacteria (purple bacteria are protobacteria that implement photosynthesis without producing oxygen), the light-harvesting complex and the RC form a compact core unit. Typical transfer times of excitations to the RC are of the order of hundreds of picoseconds. A cartoon picture of the LH1-RC complex is shown in Fig. 7. Yellow spheres represent the bacteriochlorophylls forming LH1. In the purple bacterium *Rodobacter sphaeroides*, there are 32 bacteriochlorophylls (BChl) displaced on a ring surrounding the reaction center. In Fig. 7, we display a possible structure for the RC. Instead of treating the RC as a simple two-level system, as typically done in the literature, we replace the RC with a structure containing two qubits and a d-level system, which we call a "battery." In purple bacteria, this structure has to be imagined sitting at the center of the ring. The first of these qubits [the $(N + 1)$th] interacts via coherent dipole-dipole hopping with the BChls of the ring. Excitations are then transferred at a rate γ to what we call reaction center. In turn, the RC itself is connected to larger d-level system ($d = 3$ in our simulations) via irreversible transfer at a rate γ_b. It is the interplay between the two time scales γ^{-1} and γ_b^{-1}, and their relation to the transfer efficiency, that we want to analyze here.

The master equation for the whole system is of Lindblad type: $\dot{\rho} = -i[H,\rho] + \mathcal{L}_{\text{tot}}(\rho)$. For what we said so far, the incoherent part is given by $\mathcal{L}_{\text{tot}} = \mathcal{L}_L + \mathcal{L}_{L_b} + \mathcal{L}_{\text{noise}}$ with $L = \sqrt{\gamma}\sigma_{N+1}^-\sigma_{RC}^+$ and $L_b = \sqrt{\gamma_b}\sigma_{RC}^- S_{\text{bat}}^+$. Dissipation and dephasing effects are taken into account via incoherent terms acting on the sites of the ring $\mathcal{L}_{\text{noise}} = \sum_{j=1}^N \mathcal{L}_{L_{j,\text{diss}}} + \mathcal{L}_{L_{j,\text{deph}}}$ with $L_{j,\text{diss}} = \sqrt{\gamma_{\text{diss}}}\sigma_j^-$ and $L_{j,\text{deph}} = \sqrt{\gamma_{\text{deph}}}\mathfrak{n}_j$.

Regarding the Hamiltonian of the ring degrees of freedom, we referred to the detailed structure of couplings given in Refs. 39 and 40. The most salient feature emerging from the data of Ref. 40 is that the couplings present a dimerized structure: strong coupling $t_+ = t(1 + \delta)$ alternate with weak ones $t_- = t(1 - \delta)$. Indeed, instead of using all the couplings $t_{i,j}$ reported,[40] almost the same band structure can be obtained using only a nearest-neighbor description with a dimerization of $\delta = 0.12$. Some groups have suggested the possibility that dimerization might favor the transfer efficiency.[41] Our choice of resorting to a dimerized nearest-neighbor hopping structure has the additional advantage of making the system scalable to different sizes N. Hence, our choice for the Hamiltonian is

$$H = \sum_{j=1}^N t_j(\sigma_j^-\sigma_{j+1}^+ + \sigma_j^+\sigma_{j+1}^-) + J(\sigma_j^-\sigma_{N+1}^+ + \sigma_j^+\sigma_{N+1}^-).$$

This represents N particles on a ring hopping between neighboring sites with constants $t_j = t[1 + \delta(-1)^j]$ and to a central site $N + 1$ with hopping constant J. We will also add static random diagonal noise $(H \rightarrow H + \sum_j \epsilon_j \mathfrak{n}_j)$ to inhibit the possible appearance of decoherence-free subspaces, which can limit the efficiency of transfer.[18] To be specific, we will use static random noise of the form $\sum_j t \cos(je)\mathfrak{n}_j$ where e is the Neper constant. This form of static noise mimics random noise of amplitude (variance) t and zero mean, but it has the computational advantage of being reproducible.

The results of our simulations are shown in Fig. 8. We initialize the system by starting with a pure Dicke state for the ring while keeping all other sites empty. This means the initial state is $|\psi_0\rangle = \binom{N}{n}^{-1/2}(\sigma_{\text{tot}}^+)^n|0\rangle$, where $\sigma_{\text{tot}}^+ = \sum_{j=1}^N \sigma_j^+$ refers only to the ring sites and $|0\rangle$ is the empty state for the whole system. The choice of an initial Dicke state is natural for a series of reasons. First, it allows us to treat initial states with general definite particle number $n \leq N$. Second, Dicke states are symmetric under permutation, thus carrying no net momentum. If the photon's wavelength is larger than the size of the LH1 complex, the excitations created must be a completely delocalized $k = 0$ object. In any case, since only the $k = 0$ component of the ring couples to the central $(N + 1)$th site, transfer in the antisymmetric channel $k = \pi$, being a higher-order process, is highly suppressed and gives much lower transfer efficiency.[26]

We first performed simulations on a "clean" system, i.e., with no dissipation or dephasing present. In Fig. 8, we plotted the population of the reaction center (normally called efficiency η in the literature) as a function of time for different values of γ_b. Looking at Figs. 8(a) and 8(b), the situation is completely analogous to the congestion effect observed in our simple toy model (see Figs. 2 and 3). As long as we start with a number of excitations that can be accommodated in the battery, they will all flow to the battery for $\gamma_b \neq 0$ (left panel). When we start with three particles in the ring, we see again the appearance of a nonmonotonic behavior between γ_b and γ, which shows up as a valley at large times and $\gamma_b \lesssim \gamma$ (γ_b smaller than, but of the order of γ). When we add additional decoherence in the form of dissipation and dephasing, the situation is only quantitatively changed. The valley due to the "congestion effect," although less pronounced, is still visible in Fig. 8(d).
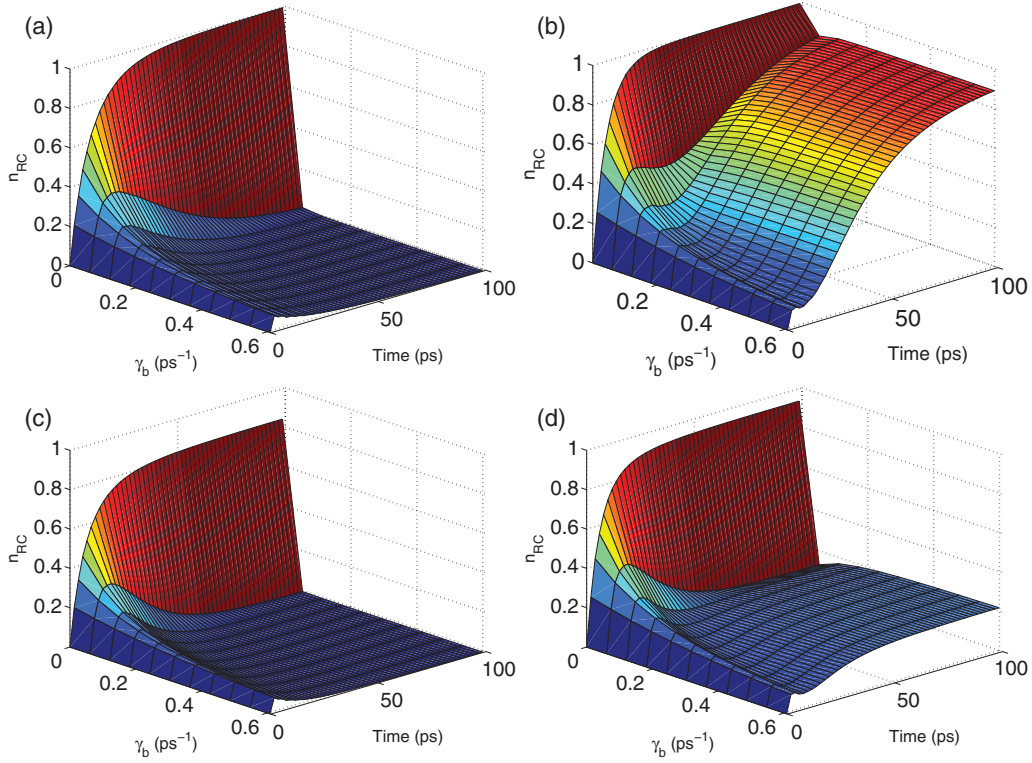
FIG. 8. (Color online) "Congestion effect" in light-harvesting complexes. The ring has $N = 4$ sites, hopping constants are $t = J = 1$ (meV) and dimerization is $\delta = 0.12$. Diagonal static noise of the form $\epsilon_n = t \cos(en)$ is added (see main text). The RC transfer rate is set to $\gamma = 0.3$ ps^{-1}. (a), (b) Clean system, no dissipation and dephasing. (c), (d) Same parameters plus dissipation and dephasing $\gamma_{\text{diss}} = \gamma_{\text{deph}} = 0.03$ ps^{-1}. (a), (c) The initial state is a two-particle Dicke state for the ring, other sites are empty. (b), (d) The initial state is a three-particle Dicke state for the ring, other sites are empty.

B. Asymptotic unitarity

To study asymptotic unitarity, the "battery" is an unnecessary complication. Therefore, we will use the same model of Fig. 7 without the battery site and the corresponding jump operator. This leads to a network of $N + 2$ qubits where the site $N + 1$ is connected to site $N + 2$ (which we called RC) via irreversible transfer at a rate γ. As done previously, we will use an n-particle Dicke state as initial state. Let us first consider the case where the only incoherent term is the one transferring particles from the central site to the RC. In this case, the dynamics becomes exactly unitary when the RC is full. Simulations on a network with $N + 2 = 6$ qubits are shown in Fig. 9. We also show the effect of dissipation and dephasing, although one order of magnitude smaller than the RC transfer. For short times, the evolution is the same as for the clean (i.e., no dissipation and dephasing) case, however, for time of order $\gamma_{\text{diss}}^{-1}$, dissipation sets in and the parametric plot for a generic matrix element $\langle n|\rho(t)|m\rangle$ spirals down to zero [Fig. 9(d)].

The conclusion of this section is as simple as it is intriguing, in view of potential applications to biological systems. If the time scale $\gamma_{\text{diss}}^{-1}$ is large enough, there may exist a time window $T_{\text{relax}} < t < \gamma_{\text{diss}}^{-1}$ in which quantum effects are not only visible but the dynamics is effectively unitary! In our models, T_{relax} is the time needed for the RC to get filled, and is of the order $T_{\text{relax}} \sim \gamma^{-1}$. Considering the LH1-RC complex, the separation of time scales does indeed occur and generally

the dissipation is four orders of magnitude smaller than the RC charge-separation rate.[26,33]

The experimental observations reported in Ref. 35 suggest that the reaction center in photosynthetic aggregates has a richer structure than usually believed. Accordingly, in place of the simple description of the RC as a sink where excitations disappear, we modeled the last part of the excitation transfer to the reaction center via an incoherent transfer between two two-level systems. This has the implication that the reaction center can not accept further excitations when it is full. Although the qubit model is clearly far from a realistic portrayal of organic chromophores, this is a plausible feature of the reaction center (see, also, Ref. 26).

C. Staircase effect

Here, we want to show that the staircase effect, studied in Sec. III, survives in more elaborate networks. We will study this effect in the model depicted in Fig. 10. To tell the truth, very similar networks as those considered here have been analyzed in the literature. The kind of networks analyzed in Ref. 19 are essentially the same as those of Fig. 10 except for the incoherent injection on the first site. In Ref. 19, the authors considered the efficiency of transfer of a single exciton localized on the leftmost site traveling toward the "trap" sitting after the rightmost site. Our modelization is the simplest one, which takes into account a continuous feeding of excitons into the network. The resulting dynamics is not constrained
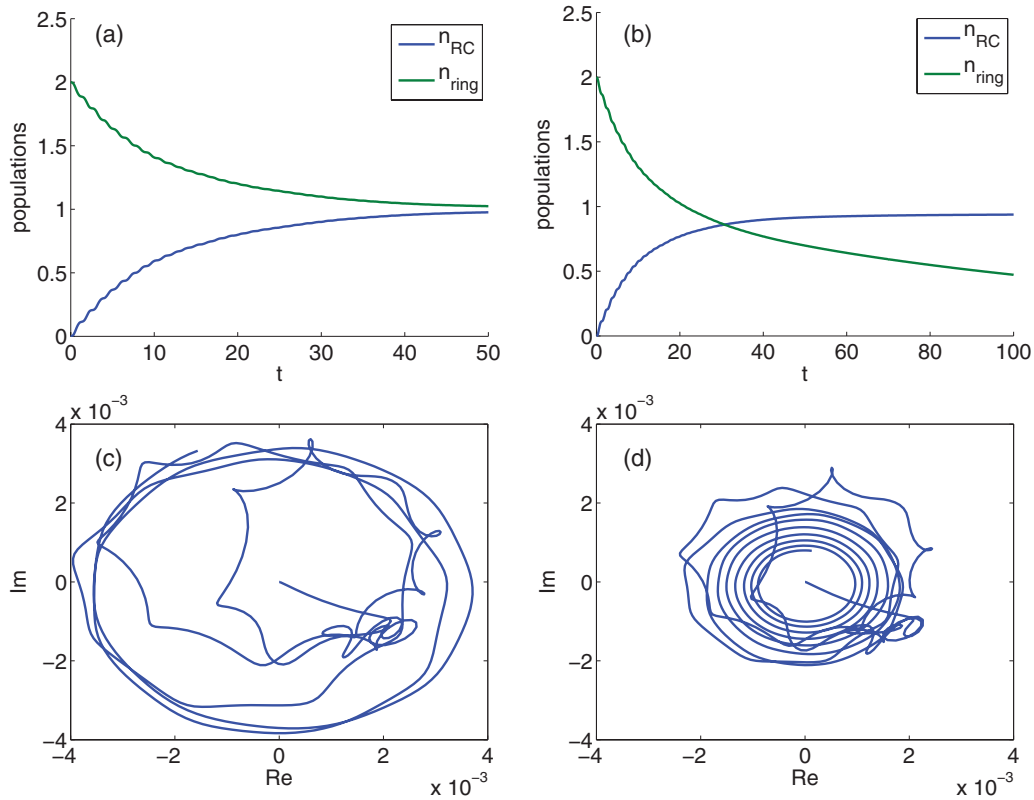
FIG. 9. (Color online) Asymptotic unitarity on a structure containing $N + 2 = 6$ sites. On (a) and (b), we plot the populations of the ring and of the RC as a function of time (arbitrary units). (c), (d) Parametric plot of the real and imaginary parts of a matrix element $\langle \psi_m | \langle 1 | \rho(t) | \psi_n \rangle | 1 \rangle$ for certain m, n. $|\psi_n\rangle$ are the Hamiltonian eigenstates. (a), (c) The Hamiltonian has $t = J = 1$, $\delta = 0.12$, diagonal static noise $\epsilon_p = t \cos(ep)$, and no dissipation or dephasing. Excitations are transferred to the RC at a rate $\gamma = 0.2$. (b), (d) Same parameters, but on the particles of the ring acts dissipation and dephasing with $\gamma_{\text{deph}} = \gamma_{\text{diss}} = 0.01$.

to any particle sector so that the simulation must necessarily be carried out in the whole Liouville space, thus making the computational cost exponential in the chain length. For this reason, we limited our simulation to open chains of $N = 6$ sites, but we have no reason to doubt that similar qualitative behavior remains for longer chains.

The model we consider consists of an open chain of N sites hopping coherently between nearest neighbors, i.e., the Hamiltonian is

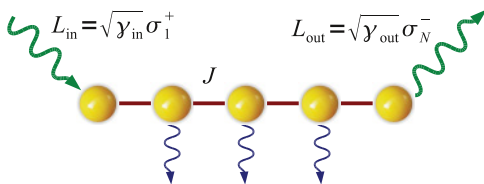$$ H = \sum_{j=1}^{N-1} J(\sigma_j^- \sigma_{j+1}^+ + \sigma_j^+ \sigma_{j+1}^-). $$

FIG. 10. (Color online) N sites interact via a nearest-neighbor hopping Hamiltonian. Particles are injected and, respectively, expelled incoherently at rates γ_{in}, γ_{out} on the first and last sites. On top of this basic structure, we can add static diagonal disorder and dissipation as well as dephasing (symbolized by thin blue wavy arrows) $\mathcal{L}_{\text{noise}} = \sum_{j=2}^{N-1} \mathcal{L}_{L_{j,\text{diss}}} + \mathcal{L}_{L_{j,\text{deph}}}$.

Particles are injected into the first site of the chain via a jump operator $L_{\text{in}} = \sqrt{\gamma_{\text{in}}} \sigma_1^+$ and taken away at the last site via $L_{\text{out}} = \sqrt{\gamma_{\text{out}}} \sigma_N^-$. On top of this basic framework, we add different layers of complexity. First, we can add some static random diagonal noise, i.e., we add site-dependent energies to the coherent part $H \to H + \sum_j \epsilon_j \mathfrak{n}_j$. Second, we can also include dissipation and dephasing acting on the inner sites of the chain by adding the following superoperator: $\mathcal{L}_{\text{noise}} = \sum_{j=2}^{N-1} \mathcal{L}_{L_{j,\text{diss}}} + \mathcal{L}_{L_{j,\text{deph}}}$ ($L_{j,\text{diss}} = \sqrt{\gamma_{\text{diss}}} \sigma_j^-$ and $L_{j,\text{deph}} = \sqrt{\gamma_{\text{deph}}} \mathfrak{n}_j$ as defined previously).

The picture that we have is the following. Through the coherent part of the evolution, excitations travel in the chain in packets of quasiparticles at velocities $v_k = O(J)$ (k is a quasimomentum label). This introduces a lag time scale $T_0 \approx L/v \sim O(L/J)$, which is the time needed for an excitation to travel from one side of the chain to the other. From Figs. 11(a)–11(f), we see that, when the population at the injection site increases, the population at the expulsion site stays constant during this time lag T_0 and vice versa.

Considering Figs. 11(c)–11(f), we can appreciate how robust the effect is with respect to various types of "perturbations." The addition of static random noise has the effect of localizing states and shuffling the single-particle dispersion ϵ_k. Both of these effects destroy the picture of wave packets traveling at constant velocity, in that both the traveling times and the dispersion of the wave packets increase. Instead, the
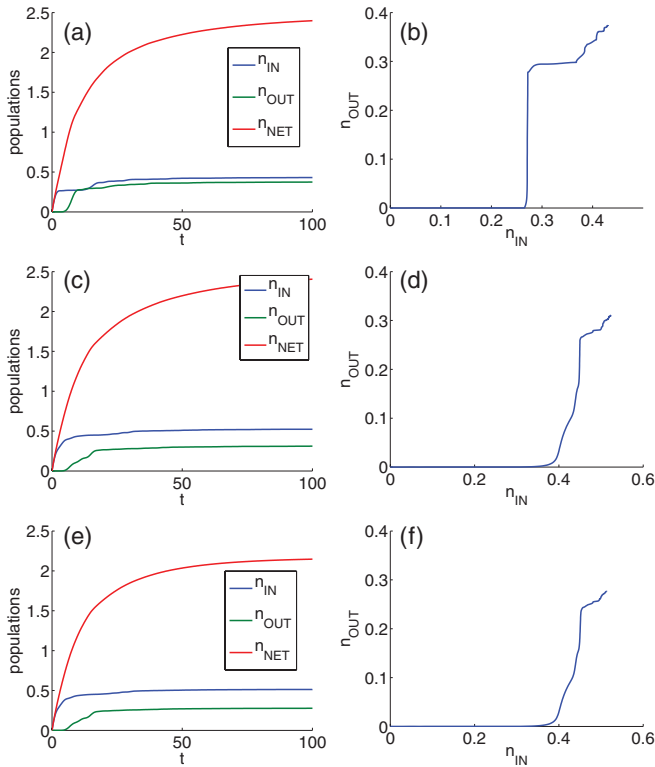
FIG. 11. (Color online) Staircase effect on an open chain of $N = 6$ sites. Parameters are $J = 1$ and $\gamma_{in} = 0.2$, $\gamma_{out} = 0.3$. n_{IN}, n_{OUT} are the populations at the injection and extraction sites, respectively, while n_{NET} is the total number of excitons in the network. (a), (b) Neither dissipation nor dephasing, and no static noise. (c), (d) Addition of diagonal static noise $\epsilon_n = J \cos(en)$. (e), (f) Static noise plus dissipation and dephasing $\gamma_{diss} = \gamma_{deph} = 10^{-2}$.

addition of dissipation (and dephasing) to the network mostly has the effect of relaxing the system at a faster rate. As long as the system has not relaxed, the effect remains visible. Comparatively, the presence of static coherent noise hinders the staircase effect more to dissipation and dephasing.

VI. CONCLUSIONS

Inspired by the models that are recently being used to describe energy transfer in photosynthetic pigments, we have identified and discussed a few effects arising in quantum networks with coherent (Hamiltonian) as well as incoherent (Lindblad) coupling between the nodes. For the reader's sake, we summarize here these basic effects.

(i) *Congestion effect.* The incoherent transfer of excitations is inversely proportional to the population in the reaction center. This is due to the hard-core nature of the excitations that effectively reduces the amplitude of the jump operator as the reaction center fills.

(ii) *Asymptotic unitarity.* Coherent, unitary evolution may emerge out of a dissipative, incoherent dynamics. This happens if states that annihilate the incoherent part of the dynamics can be reached during the time evolution. For this effect to be observable, one needs a separation of time scales $T_{relax} \ll T_{diss}$. Such separation of time scales does take place in some photosynthetic systems, e.g., in the LH1-RC complexes present in purple bacteria.

(iii) *Staircase effect.* This effect refers to a situation in which particles are injected incoherently, travel coherently along a given chain, and then are expelled (or digested) at a certain rate at the other end of the chain. The effect of the coherent part is to introduce a time scale $T_0 = O(L/v) = O(L/J)$ (L is the system size, v the velocity of excitations, and J is the energy scale of the coherent network). T_0 is roughly the time needed for the excitations to travel from one side of the chain to the other. The peculiar feature emerging from the dynamic evolution is that, when the population at the injection site increases, the population at the expulsion site stays constant during this time lag T_0 and vice versa. This effect results in a steplike behavior in the parametric plot of the injection-extraction populations. It would be interesting to see if a modification of the methods of Ref. 19, not constrained to the zero- and one-particle sectors, allows us to derive a simple classical description, i.e., a kinetic rate equation, for this effect.

The effects we analyzed in this paper can be traced back to very simple mechanisms displayed even by networks composed by only few qubits. We provided analytical solutions for these toy models and showed numerical evidence that these effects survive in more elaborate networks such as those modeling energy transfer in purple bacteria. Clearly, further investigations are in order to establish the relevance of the elementary calculations presented in this paper to the newborn field of quantum biology.

[1] R. Blankenship, *Molecular Mechanisms of Photosynthesis* (Blackwell, Malden, MA, 2002).

[2] T. Ritz, S. Park, and K. Schulten, J. Phys. Chem. B **105**, 8259 (2001).

[3] R. van Grondelle and V. Novoderezhkin, Phys. Chem. Chem. Phys. **8**, 793 (2006).

[4] J. Adolphs and T. Renger, Biophys. J. **91**, 2778 (2006).

[5] T. Renger, Photosynth. Res. **102**, 471 (2009).

[6] M. T. W. Milder, B. Brüggemann, R. van Grondelle, and J. L. Herek, Photosynth. Res. **104**, 257 (2010).

[7] T. Brixner, J. Stenger, H. M. Vaswani, M. Cho, R. E. Blankenship, and G. R. Fleming, Nature (London) **434**, 625 (2005).

[8] G. S. Engel, T. R. Calhoun, E. L. Read, T.-K. Ahn, T. Mancal, Y.-C. Cheng, R. E. Blankenship, and G. R. Fleming, Nature (London) **446**, 782 (2007).

[9]E. Collini, C. Y. Wong, K. E. Wilk, P. M. G. Curmi, P. Brumer, and G. D. Scholes, Nature (London) **463**, 644 (2010).

[10]G. Panitchayangkoon, D. Hayes, K. A. Fransted, J. R. Caram, E. Harel, J. Wen, R. E. Blankenship, and G. S. Engel, Proc. Natl. Acad. Sci. USA **107**, 12766 (2010).

[11]G. S. Schlau-Cohen, T. R. Calhoun, N. S. Ginsberg, M. Ballottari, R. Bassi, and G. R. Fleming, Proc. Natl. Acad. Sci. USA **107**, 13276 (2010).

[12]J. M. Womick, S. A. Miller, and A. M. Moran, J. Chem. Phys. **133**, 024507 (2010).

[13]K. Gaab and J. Bardeen, J. Chem. Phys. **121**, 7813 (2004).

[14]M. Mohseni, P. Rebentrost, S. Lloyd, and A. Aspuru-Guzik, J. Chem. Phys. **129**, 174106 (2008).

[15]P. Rebentrost, M. Mohseni, I. Kassal, S. Lloyd, and A. Aspuru-Guzik, New J. Phys. **11**, 033003 (2009).

[16]P. Rebentrost, M. Mohseni, and A. Aspuru-Guzik, J. Phys. Chem. B **113**, 9942 (2009).

[17]M. B. Plenio and S. Huelga, New J. Phys. **10**, 113019 (2008).

[18]F. Caruso, A. Chin, A. Datta, S. Huelga, and M. Plenio, J. Chem. Phys. **131**, 105106 (2009).

[19]J. S. Cao and R. Silbey, J. Chem. Phys. A **113**, 13825 (2009).

[20]J. Wu, F. Liu, Y. Shen, J. Cao, and R. J. Silbey, New J. Phys. **12**, 105012 (2010).

[21]A. Chin, A. Datta, F. Caruso, S. Huelga, and M. Plenio, New J. Phys. **12**, 065002 (2010).

[22]O. Mulken and T. Schmid, Phys. Rev. E **82**, 042104 (2010).

[23]H. van Amerongen, L. Valkunas, and R. van Grondelle, *Photosynthetic Excitons* (World Scientific, Singapore, 2000).

[24]J. Cao, J. Chem. Phys. **107**, 3204 (1997).

[25]T. Renger and R. Marcus, J. Chem. Phys. **116**, 9997 (2002).

[26]A. Olaya-Castro, C. F. Lee, F. F. Olsen, and N. F. Johnson, Phys. Rev. B **78**, 085115 (2008).

[27]A. Ishizaki and G. Fleming, J. Chem. Phys. **130**, 234111 (2009).

[28]S. Lloyd and M. Mohseni, New J. Phys. **12**, 075020 (2010).

[29]J. Zhu, S. Kais, P. Rebentrost, and A. Aspuru-Guzik J. Phys. Chem. B (to be published).

[30]A. Nazir, Phys. Rev. Lett. **103**, 146404 (2009).

[31]P. Nalbach, J. Eckel, and M. Thorwart, New J. Phys. **12**, 065043 (2010).

[32]F. Fassioli and A. Olaya-Castro, New J. Phys. **12**, 085006 (2010).

[33]F. Fassioli, A. Nazir, and A. Olaya-Castro, J. Phys. Chem. Lett. **14**, 2139 (2010).

[34]A. W. Roszak, T. D. Howard, J. Southall, A. T. Gardiner, C. J. Law, N. W. Isaacs, and R. J. Cogdell, Science **302**, 1969 (2003).

[35]A. B. WÃhri, G. Katona, L. C. Johansson, E. Fritz, E. Malmerberg, M. Andersson, J. Vincent, M. Eklund, M. Cammarata, M. Wulff *et al*., Science **328**, 630 (2010).

[36]G. Raszewski and T. Renger, J. Am. Chem. Soc. **130**, 4431 (2008).

[37]S. Ganapathy, G. Oostergetel, P. Wawrzyniak, M. Reus, A. Chew, F. Buda, E. Boekema, D. Bryant, A. Holzwarth, and H. de Groot, Proc. Natl. Acad. Sci. USA **106**, 8525 (2009).

[38]P. Zanardi and M. Rasetti, Phys. Rev. Lett. **79**, 3306 (1997).

[39]X. Hu, T. Ritz, A. Damjanović, and K. Schulten, J. Phys. Chem. B **101**, 3854 (1997).

[40]X. Hu and K. Schulten, Biophys. J. **75**, 683 (1998).

[41]S. Yang, D. Xu, Z. Song, and C. Sun, J. Chem. Phys. **132**, 234501 (2010).